Quantum state characterization of a fast tunable superconducting resonator

Z. L. Wang,[1] Y. P. Zhong,[1] L. J. He,[1] H. Wang,[1,a)] John M. Martinis,[2] A. N. Cleland,[2] and Q. W. Xie[3]
[1]*Department of Physics, Zhejiang University, Hangzhou 310027, China*
[2]*Department of Physics, University of California, Santa Barbara, California 93106, USA*
[3]*Toyota Technological Institute, Nagoya, Aichi 468-8511, Japan*

(Received 10 January 2013; accepted 9 April 2013; published online 24 April 2013)

We demonstrate a frequency-tunable superconducting coplanar waveguide resonator, with a tuning range of half a gigahertz and a switching time of 1 ns. The resonator is made tunable by inserting a superconducting quantum interference device in the center strip of the resonator. Quantum measurements are made by probing the resonator with a superconducting qubit, allowing us to use microwave photon Fock states to benchmark the resonator performance. Using the resonator, we shuttle energy quanta between the qubit and a microscopic two-level state. The tunable resonator can, therefore, serve as a communication bus or memory element in a prototype quantum processor. © *2013 AIP Publishing LLC*. [http://dx.doi.org/10.1063/1.4802893]

Superconducting resonators have played an important role in quantum computation and information processing research.[1,2] Resonators have been used to protect superconducting qubits from a noisy environment and to dispersively detect qubit states;[3–5] to shuttle energy quanta between qubits, enabling macroscopic entanglement;[6–8] and to couple different types of quantum systems, forming hybrid quantum devices.[9–11] Recently, significant progress has been made in manipulating complex photon states in such resonators as well as creating macroscopic quantum entanglement.[12,13] Circuits using resonators as quantum memories and as quantum communication buses have allowed the demonstration of a quantum von Neumann architecture[14] and factoring the number 15 using Shor's algorithm.[15] This type of architecture, in which the qubits are complemented by memory resonators and coupled to one another via a resonator bus, was shown[16] to provide sufficient performance for medium-scale quantum information processing.

Most of these experiments were performed using resonators that could only operate at a fixed resonance frequency. Significant additional flexibility can, however, be achieved using tunable resonators, giving more latitude in the operation of quantum gates, avoiding "holes" in the qubit and resonator T_1 spectra, and circumventing microscopic two-level states (TLSs). As observed experimentally, the frequency distribution of TLS defects is random and non-static,[17] and circuit performance can be strongly affected by a nearby TLS.

The resonance frequency of superconducting resonators can be tuned by inserting a superconducting quantum interference device (SQUID) in the resonator and tuning with a magnetic field.[18,19] Such a scheme has been used for signal amplification,[19] for coupling spin ensembles,[11] and for testing fundamental physics.[20] However, single-photon control, complementary to that achieved with qubits and which is relevant to quantum information applications, has not been demonstrated using a frequency-tunable superconducting resonator.

Here, we demonstrate the fast frequency-tuning of a superconducting coplanar waveguide (CPW) resonator, with a tuning range of more than half a gigahertz. The resonator is capacitively coupled to a superconducting phase qubit, allowing single-photon experiments. We use the resonator to demonstrate quantum-coherent frequency-tuning of one- and two-photon Fock states and also use the resonator as an intermediary in the transfer of quantum states between the qubit and a spurious microscopic two-level state.

Our sample consists of a half-wavelength ($\lambda/2$) CPW microwave resonator, with a SQUID inserted in the middle of the resonator transmission line (see Fig. 1(a)); a phase qubit is capacitively coupled to one end of the resonator. A schematic circuit diagram is shown in Fig. 1(b). The SQUID can be viewed as a lumped-element inductor with a variable inductance $L_s(\Phi) = \Phi_0/[4\pi I_c|\cos(\pi\Phi/\Phi_0)|]$, where Φ is the applied magnetic flux, $\Phi_0 = h/2e$ is the magnetic flux quantum, and I_c is the critical current of each SQUID junction. The SQUID inductance can be varied by applying an external magnetic field. For moderate detunings, the resonance frequency f_r of the resonator can be well approximated[18] by $f_r(\Phi) = f_0/[1 + L_s(\Phi)/L\ell]$, where $f_0 = (2\sqrt{LC}\ell)^{-1}$, L and C are the inductance and capacitance per unit length of the transmission line, and ℓ is the length of the transmission line.

Measurements were performed at 20 mK in a cryogen-free dilution refrigerator (Leiden CF450). The phase qubit had an energy lifetime $T_{1q} = 400$ ns and phase coherence time $T_{2q} \approx 100$ ns at its idle point of 6.39 GHz. By applying a spin echo pulse, the dephasing time could be improved to $T_{2q}^{*} \approx 400$ ns. We used qubit spectroscopy to characterize the qubit-resonator interaction, as described elsewhere.[12] The resonance frequency of the resonator with zero applied magnetic field was around 6.9 GHz, with a qubit-resonator coupling strength of 25 MHz, consistent with the designed coupling capacitance of 2 fF. We characterized the magnetic field tuning of the resonator using the pulse sequence shown in Fig. 1(c) inset; the results are shown in Fig. 1(c). The data (dots) agree well with the calculated response (line) over the tuning range of about 670 MHz. From this measurement, the

a)Electronic mail: hhwang@zju.edu.cn

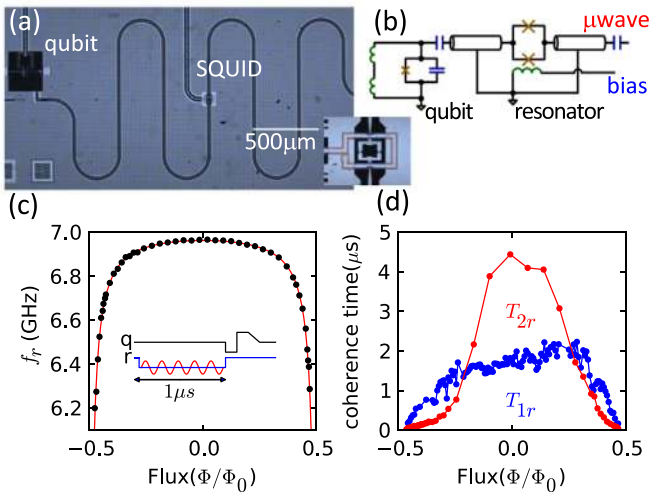

FIG. 1. Geometry and characterization of the tunable resonator. (a) Optical micrograph of the circuit. The SQUID tuner (detailed in the bottom-right panel) is inserted in the middle of the CPW transmission line. The size of the SQUID loop is approximately $26\mu m \times 22\mu m$. (b) Simplified schematic circuit diagram for the device. (c) Measured resonator frequency as a function of magnetic flux coupled to the SQUID loop (dots) and fit according to theory (line). Inset is the pulse sequence. We excited the resonator with a 1 μs-long microwave tone (the red sinusoidal) at various frequencies in the 6–7 GHz range while the resonator SQUID was at a fixed flux value (the blue line), and then swapped the excitation into the qubit for readout (the black line). The excitation in the resonator was swapped into the qubit by tuning the two into resonance for a fixed amount of time. The trapezoid pulse at the end of the pulse sequence was to readout the qubit $|e\rangle$ probability. The microwave frequency value corresponding to the maximum qubit response was chosen as the resonator resonance frequency at this SQUID flux. (d) Resonator T_{1r} and T_{2r} as a function of applied magnetic flux in SQUID.

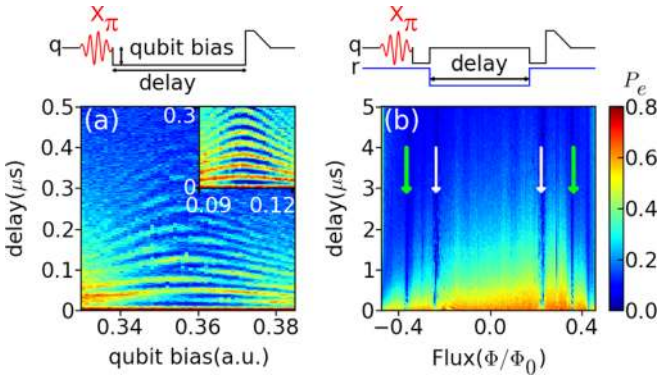

FIG. 2. (a) Swap spectroscopy for a qubit capacitively coupled to a non-tunable CPW resonator. Pulse sequence at top: we excited the qubit with a π pulse (red), tuned the qubit frequency close to the resonator by changing the qubit bias, then after a delay, measured the qubit excited state. Main plot shows $|e\rangle$ probability P_e (color scale) versus delay and qubit bias. Inset displays same data for a qubit-resonator swap spectrum in the absence of a TLS, with a Lorentzian-shaped chevron with clear and continuous swap dependence on qubit frequency; main panel shows the perturbation of the chevron due to the TLS. (b) Single-photon energy dissipation of tunable resonator in Fig. 1. Pulse sequence at top: we excited the qubit and immediately swapped the excitation into the resonator, then tuned the resonator frequency by changing the flux applied to the embedded SQUID. After a delay time, we swapped the residue excitation from resonator to qubit for measurement. Main panel: measured excited state probability P_e typically decays exponentially with time, with decay time T_{1r}. Arrows indicate chevron-like features consistent with the resonator swapping energy with a defect TLS.

critical current of each Josephson junction in the SQUID is estimated to be about 2.7 μA.

Using the qubit to swap single photons into and out of the resonator, we obtained the resonator's single-photon T_{1r} and T_{2r} at different flux bias points (Fig. 1(d)). At small flux bias, the resonator T_{1r} is approximately 2.3 μs and T_{2r} is almost T_{1r}-limited, comparable to the performance of CPW resonators without SQUIDs.[8] The decrease of T_{1r} and T_{2r} with applied magnetic field is consistent with the presence of a dissipation channel associated with the SQUID, which will be discussed elsewhere. We note that T_{2r} away from zero flux can be enhanced by performing a dynamic decoupling sequence (data not shown). We mainly operated the resonator at small bias, corresponding to a tuning range of $\sim$100 MHz, where both T_{1r} and T_{2r} are significantly larger than the on-resonance gate operation times.

The phase qubit couples strongly to spurious TLS at certain qubit frequencies; these TLS are thought to be atomic-size defects in the tunnel junction barrier or other dielectrics in the circuit.[21] These TLS are most apparent when they generate Lorentzian features in the real-time swap spectroscopy of the qubit. Swap spectroscopy was performed by preparing the qubit in its $|e\rangle$ state, tuning it to a certain frequency, and monitoring the qubit T_{1q} decay time as a function of the qubit frequency. This measurement gives information about the qubit's environment, yielding, for example, the frequencies and lifetimes of strongly coupled TLS. In Fig. 2(a), we show a measurement on a sample in which a phase qubit is capacitively coupled to a fixed-frequency CPW resonator—an unlucky case where a TLS appears right near the resonance frequency of the resonator, distorting the usual Lorentzian form of the energy swapping between the qubit and the resonator. The existence of such TLS, either directly coupled to the resonator or to the qubit, causes unpredictable dispersive phase shifts and energy absorption, reducing the fidelity of quantum gates.

In Fig. 2(b), we display the results of a measurement similar to that shown in Fig. 2(a), but tuning the resonator frequency instead of the qubit frequency. We excited the resonator to the $n = 1$ Fock state using the qubit, tuned the resonator to a particular frequency, and measured its T_{1r} decay time as a function of its frequency. Two-level states again appear as Lorentzian features (arrows in Fig. 2(b)). These TLS can again cause problems with gate fidelity and visibility, and having the freedom to tune the resonator away from these features can improve gate performance.

In Fig. 3, we demonstrate this additional freedom, showing three different methods for transferring photon Fock states between the qubit and the resonator. In Fig. 3(a), we tuned the qubit while keeping the resonator frequency fixed; in Fig. 3(b), we tuned the resonator while keeping the qubit fixed; and in Fig. 3(c), we tuned both the qubit and resonator to an optimal frequency. In Fig. 3(a), where we kept the resonator frequency at its unbiased value, a TLS that happened to be close to this frequency generated a small modulation of the qubit-resonator swapping amplitude for the $n = 1$ Fock state, probably due to some state amplitude swapping into the TLS. The modulation in amplitude is consistent with roughly 5% of the energy being transferred to the TLS. By biasing the resonator frequency away from the TLS, as in Fig. 3(c), this unwanted modulation was much less apparent. The increase of $\sim$10% in the amplitude of the vacuum Rabi

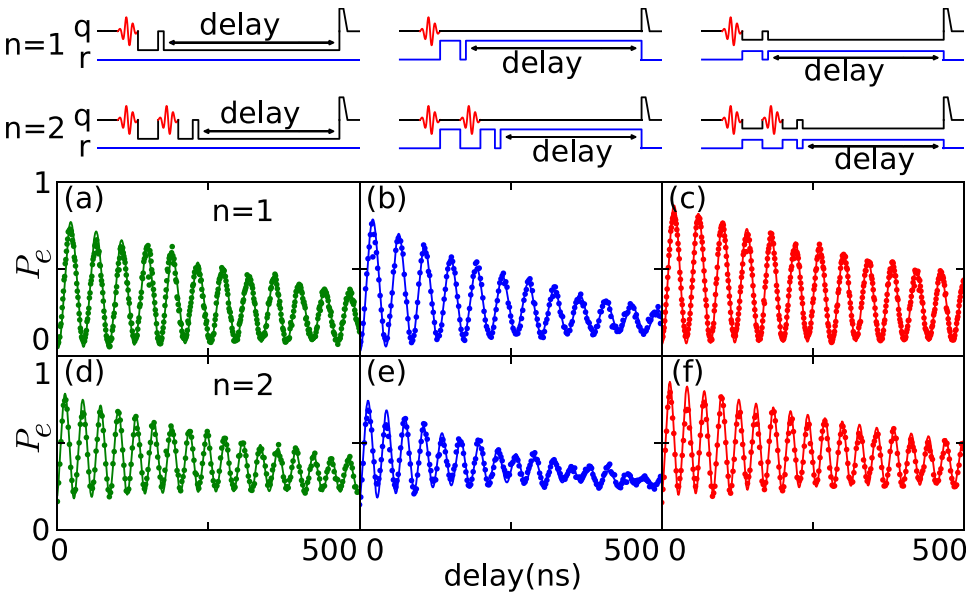

FIG. 3. Benchmark test of the tunable resonator using the $n=1$ and $n=2$ photon Fock states. The resonator Fock state was generated and probed by (a) and (d) biasing the qubit to the resonator frequency, (b) and (e) biasing the resonator to the qubit frequency, or (c) and (f) biasing both to a sweet frequency point. Shown are the qubit probabilities versus the interaction time for reading out the Fock state (lines are guides to the eye). Schematics of the measurement sequences are shown on top. Red sine waves are π pulses to excite the qubit. Black and blue lines are the qubit flux bias and the resonator SQUID bias used to change their frequencies, respectively. It is seen that biasing both the qubit and the resonator (c) and (f) gives the best result.

oscillations in Fig. 3(c) compared to Fig. 3(a) illustrates the value in choosing an optimal operating point for both the qubit and the resonator.

We further tested the device using the $n=2$ Fock state, as shown in Figs. 3(d)–3(f). A clear improvement in the swap amplitude is again seen at the optimal operating point. We emphasize that in this case, to avoid the TLS interference, we only need to slightly tune the resonator from its unbiased point, preserving its T_{1r} and T_{2r}.

We can look in more detail at the TLS features shown in Fig. 2(b). For example, when the resonator was tuned to 6.85 GHz by biasing its SQUID at $\Phi/\Phi_0 = 0.364$, the resonator was found to swap energy with a TLS with a coupling strength of 5.49 MHz, as shown in Fig. 4(a). The qubit was found to have a much weaker coupling with this particular TLS, as indicated by the arrow in Fig. 4(b). The swapping feature in this figure was almost undetectable when the resonator was detuned far from the TLS (data not shown), suggesting that this TLS is physically proximate to the resonator. Using the strong coupling to the resonator, we were able to perform quantum experiments using the TLS. We first placed the qubit in its excited state $|e\rangle$, transferred the energy quantum into the resonator, and then swapped this excitation into the TLS by tuning the resonator to the TLS frequency. After storing the energy quantum in the TLS for a delay time, we performed a swap back to the resonator, then to the qubit for measurement. The measured qubit excited-state probability versus delay time in the TLS gives the TLS energy lifetime $T_{1t} = 380$ ns (Fig. 4(c)). Using a similar sequence, we transferred the superposition state $(|g\rangle + |e\rangle)/\sqrt{2}$ from the qubit to the resonator to the TLS, and then retrieved it for measurement, which yielded the TLS phase coherence time $T_{2t} = 740$ ns (Fig. 4(d)). We see that $T_{2t} \approx 2T_{1t}$, so the energy lifetime determines T_{2t}. We emphasize that the qubit cannot directly access this TLS without the assistance of the tunable resonator, as this TLS does not couple directly to the qubit. These quantum operations, therefore, illustrate the use of the tunable resonator as a fast and switchable quantum bus.

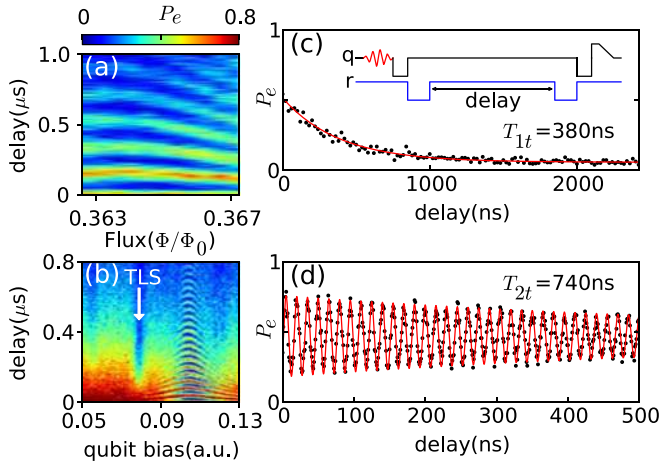

FIG. 4. Coherent control of a microscopic TLS via the tunable resonator. (a) Resonator real-time swap spectroscopy showing its interaction with a TLS through the partial Lorentzian pattern. The TLS generates a resonance at 6.85 GHz, as estimated from the resonator frequency at its SQUID bias $\Phi/\Phi_0 = 0.364$. The same feature is also observable in Fig. 2(b) (indicated by the green arrow). Its coupling strength to the resonator is 5.49 MHz using a 182 ns 2π-swaptime estimated from the figure. (b) Qubit real-time swap spectroscopy. The Lorentzian feature represents its interaction with the resonator. The qubit is also very weakly coupled to a TLS (indicated by the white arrow) via the resonator-TLS coupling shown in (a). (c) Measurement of the TLS lifetime via the resonator. Inset: Pulse sequence. (d) Measurement of the TLS dephasing time.

In conclusion, we have demonstrated a rapidly tunable resonator with a frequency tuning range of more than half a gigahertz. We have performed one- and two-photon swaps between the qubit and the resonator, and swaps between the qubit and a TLS via the resonator. We believe that this kind of tunable resonator could be very useful in quantum information circuits and may also stimulate new ideas[22] for the use of resonators in quantum computation and simulation.

This work was supported by the National Basic Research Program of China (2012CB927404), the National Natural Science Foundation of China (11174248, 11222437, and 11104242), Zhejiang Provincial Natural Science Foundation of China (LR12A04001), and by IARPA under ARO Award No. W911NF-08-01-0336 and under ARO Award No.

W911NF-09-1-0375 of USA. Z.L.W. acknowledges partial support by the Scientific Research Fund of Zhejiang Provincial Education Department (Y200909427). Devices were made at the UC Santa Barbara Nanofabrication Facility, a part of the NSF funded National Nanotechnology Infrastructure Network.

[1]J. You and F. Nori, Phys. Today **58**(11), 42 (2005).
[2]J. Clarke and F. Wilhelm, Nature **453**, 1031 (2008).
[3]A. Wallraff, D. I. Schuster, A. Blais, L. Frunzio, R. S. Huang, J. Majer, S. Kumar, S. M. Girvin, and R. J. Schoelkopf, Nature **431**, 162 (2004).
[4]M. Reed, L. DiCarlo, B. Johnson, L. Sun, D. Schuster, L. Frunzio, and R. Schoelkopf, Phys. Rev. Lett. **105**, 173601 (2010).
[5]P. J. Leek, M. Baur, J. M. Fink, R. Bianchetti, L. Steffen, S. Filipp, and A. Wallraff, Phys. Rev. Lett. **104**, 100504 (2010).
[6]M. A. Sillanpaa, J. I. Park, and R. W. Simmonds, Nature **449**, 438 (2007).
[7]J. Majer, J. Chow, J. Gambetta, J. Koch, B. Johnson, J. Schreier, L. Frunzio, D. Schuster, A. Houck, A. Wallraff, A. Blais, M. H. Devoret, S. M. Girvin, and R. J. Schoelkopf, Nature **449**, 443 (2007).
[8]M. Ansmann, H. Wang, R. C. Bialczak, M. Hofheinz, E. Lucero, M. Neeley, A. D. O'Connell, D. Sank, M. Weides, J. Wenner, A. N. Cleland, and J. M. Martinis, Nature **461**, 504 (2009).
[9]D. I. Schuster, A. P. Sears, E. Ginossar, L. DiCarlo, L. Frunzio, J. J. L. Morton, H. Wu, G. A. D. Briggs, B. B. Buckley, D. D. Awschalom, and R. J. Schoelkopf, Phys. Rev. Lett. **105**, 140501 (2010).
[10]Y. Kubo, F. R. Ong, P. Bertet, D. Vion, V. Jacques, D. Zheng, A. Dréau, J.-F. Roch, A. Auffeves, F. Jelezko, J. Wrachtrup, M. F. Barthe, P. Bergonzo, and D. Esteve, Phys. Rev. Lett. **105**, 140502 (2010).
[11]Y. Kubo, C. Grezes, A. Dewes, T. Umeda, J. Isoya, H. Sumiya, N. Morishita, H. Abe, S. Onoda, T. Ohshima, V. Jacques, A. Dréau, J.-F. Roch, I. Diniz, A. Auffeves, D. Vion, D. Esteve, and P. Bertet, Phys. Rev. Lett. **107**, 220501 (2011).
[12]M. Hofheinz, H. Wang, M. Ansmann, R. C. Bialczak, E. Lucero, M. Neeley, A. D. O'Connell, D. Sank, J. Wenner, J. M. Martinis, and A. N. Cleland, Nature **459**, 546 (2009).
[13]H. Wang, M. Mariantoni, R. C. Bialczak, M. Lenander, E. Lucero, M. Neeley, A. D. O'Connell, D. Sank, M. Weides, J. Wenner, T. Yamamoto, Y. Yin, J. Zhao, J. M. Martinis, and A. N. Cleland, Phys. Rev. Lett. **106**, 060401 (2011).
[14]M. Mariantoni, H. Wang, T. Yamamoto, M. Neeley, R. C. Bialczak, Y. Chen, M. Lenander, E. Lucero, A. D. O'Connell, D. Sank, M. Weides, J. Wenner, Y. Yin, J. Zhao, A. N. Korotkov, A. N. Cleland, and J. M. Martinis, Science **334**, 61 (2011).
[15]E. Lucero, R. Barends, Y. Chen, J. Kelly, M. Mariantoni, A. Megrant, P. O'Malley, D. Sank, A. Vainsencher, J. Wenner, T. White, Y. Yin, A. N. Cleland, and J. M. Martinis, Nat. Phys. **8**, 719 (2012).
[16]A. Galiautdinov, A. N. Korotkov, and J. M. Martinis, Phys. Rev. A **85**, 042321 (2012).
[17]Y. Shalibo, Y. Rofe, D. Shwa, F. Zeides, M. Neeley, J. M. Martinis, and N. Katz, Phys. Rev. Lett. **105**, 177001 (2010).
[18]M. Sandberg, C. M. Wilson, F. Persson, T. Bauch, G. Johansson, V. Shumeiko, T. Duty, and P. Delsing, Appl. Phys. Lett. **92**, 203501 (2008).
[19]T. Yamamoto, K. Inomata, M. Watanabe, K. Matsuba, T. Miyazaki, W. D. Oliver, Y. Nakamura, and J. S. Tsai, Appl. Phys. Lett. **93**, 042510 (2008).
[20]C. Wilson, G. Johansson, A. Pourkabirian, M. Simoen, J. Johansson, T. Duty, F. Nori, and P. Delsing, Nature **479**, 376 (2011).
[21]J. M. Martinis, K. B. Cooper, R. McDermott, M. Steffen, M. Ansmann, K. D. Osborn, K. Cicak, S. Oh, D. P. Pappas, R. W. Simmonds, and C. C. Yu, Phys. Rev. Lett. **95**, 210503 (2005).
[22]F. W. Strauch, Phys. Rev. Lett. **109**, 210501 (2012).